


# Structure of the murine CD94–NKG2A receptor in complex with Qa-1<sup>b</sup> presenting an MHC-I leader peptide

Bruce J. MacLachlan<sup>1</sup>, Lucy C. Sullivan<sup>2</sup>, Andrew G. Brooks<sup>2</sup>, Jamie Rossjohn<sup>1,3</sup> and Julian P. Vivian<sup>1,\*</sup> 

<sup>1</sup> Infection and Immunity Program and Department of Biochemistry and Molecular Biology, Biomedicine Discovery Institute, Monash University, Clayton, Australia

<sup>2</sup> Department of Microbiology and Immunology, Peter Doherty Institute for Infection and Immunity, The University of Melbourne, Parkville, Australia

<sup>3</sup> Institute of Infection and Immunity, School of Medicine, Cardiff University, UK

## Keywords

immune checkpoint molecules; immune system; inhibitory membrane receptors; MHC-class I; natural killer cell education

## Correspondence

A. G. Brooks, Department of Microbiology and Immunology, Peter Doherty Institute for Infection and Immunity, The University of Melbourne, Parkville, Vic. 3010, Australia  
 Tel: +61 3 8344 9925

E-mail: [agbrooks@unimelb.edu.au](mailto:agbrooks@unimelb.edu.au) and

J. Rossjohn and J. P. Vivian, Infection and Immunity Program and Department of Biochemistry and Molecular Biology, Biomedicine Discovery Institute, Monash University, Clayton, Vic. 3800, Australia  
 Tel: +61 3 990 2925, Tel: +61 3 9231 2632  
 E-mail: [jamie.rossjohn@monash.edu](mailto:jamie.rossjohn@monash.edu) (JR); [jvivian@svi.edu.au](mailto:jvivian@svi.edu.au) (JPV)

## Present address

\*St. Vincent's Institute of Medical Research, Fitzroy, Australia

(Received 23 October 2023, revised 26 November 2023, accepted 27 December 2023)

doi:10.1111/febs.17050

The heterodimeric natural killer cells antigen CD94 (CD94)–NKG2A/NKG2-B type II integral membrane protein (NKG2A) receptor family expressed on human and mouse natural killer (NK) cells monitors global major histocompatibility complex (MHC) class I cell surface expression levels through binding to MHC class Ia-derived leader sequence peptides presented by HLA class I histocompatibility antigen, alpha chain E (HLA-E; in humans) or H-2 class I histocompatibility antigen, D-37 (Qa-1<sup>b</sup>; in mice). Although the molecular basis underpinning human CD94–NKG2A recognition of HLA-E is known, the equivalent interaction in the murine setting is not. By determining the high-resolution crystal structure of murine CD94–NKG2A in complex with Qa-1<sup>b</sup> presenting the Qa-1 determinant modifier peptide (QDM), we resolved the mode of binding. Compared to the human homologue, the murine CD94–NKG2A–Qa-1<sup>b</sup>–QDM displayed alterations in the distribution of interactions across CD94 and NKG2A subunits that coincide with differences in electrostatic complementarity of the ternary complex and the lack of cross-species reactivity. Nevertheless, we show that Qa-1b could be modified through W65R + N73I mutations to mimic HLA-E, facilitating binding with both human and murine CD94–NKG2A. These data underscore human and murine CD94–NKG2A cross-species heterogeneity and provide a foundation for humanising Qa-1b in immune system models.

## Abbreviations

ADCC, antibody-dependent cellular cytotoxicity; EGFR, epidermal growth factor receptor; HLA, human leukocyte antigen; ITIM, immunoreceptor tyrosine-based inhibitory motif; MHC, major histocompatibility complex; NK, natural killer; PBMC, peripheral blood mononuclear cells; pMHC, peptide-major histocompatibility complex; QDM, Qa-1 determinant modifier; SPR, surface plasmon resonance; TCR, T cell receptor; TGF-β, transforming growth factor-β.

## Introduction

Natural killer (NK) and T cells express an array of receptors that sense and respond to major histocompatibility complex (MHC) molecules expressed across all nucleated cell types. Many of these receptors, expressing the common immunoreceptor tyrosine-based inhibitory motifs (ITIM) [1], modulate NK and T-cell activity through engagement to their MHC ligands resulting in inhibition of effector function – such as directed cell lysis in NK and CD8<sup>+</sup> T cells [2,3]. These receptors function to limit autoimmunity and over-reactivity to antigen and serve as a mechanism by which interference with MHC-driven immunity by viruses and tumours can be detected, i.e. ‘missing self’ by NK cells [4].

One such molecule expressed by mature NK and activated T cells is NKG2A that assembles with CD94 to form an inhibitory heterodimeric receptor [2,5]. CD94 and NKG2A are ancient lineages of C-type lectins, with homologues identified in some nonvertebrate species [6] and homologues found across all vertebrate species including in mouse [7]. CD94–NKG2A heterodimers are known to bind HLA-E [5] in humans, and Qa-1<sup>b</sup> in mouse [8] – the equivalent MHC homologue. Through this interaction, CD94–NKG2A mediated inhibition serves to educate NK cells, to tune NK cell activation and prevent NK cell activity against HLA-E/Qa-1<sup>b</sup> that is broadly expressed by healthy nucleated cells [5,9]. HLA-E/Qa-1<sup>b</sup> itself presents peptides derived from leader sequences of classical MHC-I molecules and thus acts as a monitor for the global expression of MHC-I [10]. As such, reduced MHC-I expression and consequent HLA-E/Qa-1<sup>b</sup> surface loss, such as through viral immunomodulation, can unleash NK cell degranulation and targeted cell lysis. Consequently, viruses have evolved strategies to preserve HLA-E expression to inhibit NK cell activity such as by human cytomegalovirus (HCMV) where the protein UL40 encodes leader sequences which acts as a peptide ligand for HLA-E [11]. Therapeutically, targeting of NKG2A/Qa-1<sup>b</sup> can enhance NK cell cytotoxicity and decrease viral antigen titre in a murine model of chronic hepatitis B infection [12].

In addition to a role in NK cell immunity, CD94–NKG2A is also expressed by activated/exhausted T cells in response to chronic antigen stimulation [13] or tumour infiltration [14]. Here, CD94–NKG2A limits sustained CD8<sup>+</sup> T-cell effector function [3] and can be upregulated under suppressive cytokines such as TGF-β [15,16]. Similarly, HLA-E/Qa-1<sup>b</sup> over-expression by tumour cells has been attributed to enhanced tumourigenicity through appropriation of such mechanisms [17]. Thus HLA-E expression is a negative prognostic marker for breast cancer [18].

Conversely, loss of HLA-ABC expression on bladder tumours is countered by acquired expression of NKG2A<sup>+</sup> on CD8<sup>+</sup> T cells; where NKG2A blockade can boost an anti-tumour TCR-independent response [19]. Targeting of the CD94–NKG2A–Qa-1<sup>b</sup>/HLA-E axis in onco-immunotherapy has shown promising efficacy. For example, PD(L)-1 and NKG2A blockade combination therapy increases survival in pre-clinical tumour models [20]. In humans, combination therapy of NKG2A blockade with cetuximab (an EGFR-depleting antibody) in individuals with squamous cell carcinoma of the head and neck exhibited increased response rates compared to those previously reported for cetuximab therapy alone [20]. Such activity was attributed to enhanced ADCC activity by NKG2A<sup>+</sup> NK cells. Similarly, targeting of the CD94–NKG2A–Qa-1<sup>b</sup> axis during peptide vaccination, which induced NKG2A expression on CD8<sup>+</sup> T cells, improved treatment efficacy in murine vaccine models [21].

HLA-E and Qa-1<sup>b</sup> both present highly similar peptides in highly homologous conformations [22]. Despite this, human CD94–NKG2A exhibits no cross-species binding to HLA-E-VMA or Qa-1<sup>b</sup>-Qdm in surface plasmon resonance experiments [22]. Similarly, Qa-1<sup>b</sup>-Qdm tetramers do not stain human PBMC nor do HLA-E-VMA tetramers bind murine splenocytes [23]. However, detectable binding of HLA-E-VMA tetramers to Rhesus PBMC highlights a divergence in CD94–NKG2A interactions with MHCs at least between primates and mouse [23].

As a result of the increasing interest in NKG2A as a target for immune therapies, understanding of CD94–NKG2A function in pre-clinical animal models is of increasing importance. Whilst a structural understanding of Qa-1<sup>b</sup> exists, structural data describing CD94–NKG2A heterodimeric assembly and its engagement to Qa-1<sup>b</sup> remains unsolved. To this end, we crystallised murine CD94–NKG2A in complex with Qa-1<sup>b</sup> presenting the Qa-1 determinant modifier (Qdm) peptide (AMAPRTLTL) – the most abundant peptide eluted from Qa-1<sup>b</sup> molecules. The resultant crystal structure describes how CD94–NKG2A assembles to engage Qa-1<sup>b</sup> in a similar overall fashion to the human homologue, yet subtle differences at the receptor-ligand interface underscore differences in recognition.

## Results

### Crystal structure of murine CD94–NKG2A in complex with Qa-1<sup>b</sup>-Qdm

We determined the structure of murine CD94–NKG2A (henceforth mCD94 & mNKG2A) in complex with Qa-

**Table 1.** Data collection and refinement statistics.

Data collection statistics	CD94–NKG2A/Qa-1 <sup>b</sup> -Qdm
Temperature (K)	100
X-ray source	MX2 Australian synchrotron
Space group	<i>P</i> <sub>2</sub> <i>1</i> <sub>2</sub> <i>1</i>
Cell dimensions	<i>a</i> = 52.2, <i>b</i> = 65.1, <i>c</i> = 198.6
Resolution Å	50.0–2.60 (2.74–2.60)
Total no. observations	21 632 (12725)
No. unique observations	12 620 (3077)
Multiplicity	8.0 (8.2)
Data completeness (%)	100 (100)
1/ $\sigma_1$	11.8 (1.9)
<i>R</i> <sub>merge</sub> (%) <sup>1</sup>	0.12 (0.82)
Refinement statistics	
Non-hydrogen atoms	5141
Protein	5040
Water	101
<i>R</i> <sub>factor</sub> (%) <sup>2</sup>	20.6
<i>R</i> <sub>free</sub> (%) <sup>2</sup>	25.1
r.m.s.d. from ideality	
Bond lengths (Å)	0.008
Bond angles (°)	1.03
Ramachandran plot	
Favoured regions (%)	95.5
Allowed regions (%)	4.5
B-factors (Å <sup>2</sup> )	
Average main chain	63
Average side chain	69
Average water	52

<sup>1</sup> $R_{\text{merge}} = \sum_{\text{hkl}} \sum_j |I_{\text{hkl},j} - \langle I_{\text{hkl}} \rangle| / \sum_{\text{hkl}} \sum_j I_{\text{hkl},j}$ ; <sup>2</sup> $R_{\text{factor}} = \sum_{\text{hkl}} \|F_o - |F_c|\| / \sum_{\text{hkl}} |F_o|$  for all data excluding the 5% that comprised the *R*<sub>free</sub> used for cross-validation.

1<sup>b</sup> loaded with the Qa-1 determinant modifier (Qdm/H-2D<sub>3–11</sub>; AMAPRTL<sub>11</sub>) peptide. Each component was expressed, refolded and purified from *Escherichia coli* produced inclusion bodies and crystallised in complex in 23% PEG3350 and 0.2 M NaBr. mCD94–NKG2A–Qa-1<sup>b</sup>-Qdm crystallised in space group *P*<sub>2</sub>*1*<sub>2</sub>*1* (cell dimensions *a* = 52.2, *b* = 65.1, *c* = 198.6), diffracted to 2.6 Å resolution and the consequent structure refined to a *R*<sub>factor</sub> and *R*<sub>free</sub> of 20.6% and 25.1%, respectively (Table 1). The quality of the electron density at the interface of CD94–NKG2A with Qa-1<sup>b</sup> was of high quality, allowing for robust interpretation of the structure.

Analysis of the murine CD94–NKG2A–Qa-1<sup>b</sup>-Qdm complex structure revealed that mCD94–NKG2A formed a heterodimer that bound near-perpendicular atop the Qa-1<sup>b</sup> binding groove (Fig. 1A). Ligand binding by mCD94–NKG2A across the peptide binding groove resulted in mCD94 and mNKG2A binding predominantly over the  $\alpha$ 1 and  $\alpha$ 2 helices of Qa-1<sup>b</sup>, respectively (Fig. 1B). This locale positioned mNKG2A over the N-terminal portion of Qdm (peptide residues P1–5) with the mCD94 subunit binding over the exposed central peptide portion (P5–6) (Table 2).

The mCD94–NKG2A heterodimer assembled in the same manner as the previously solved human homologue structure [24], characterised by three  $\beta$ -strands from each c-type lectin fold subunit (NKG2A- $\beta$ 1, - $\beta$ 2, - $\beta$ 7 and CD94- $\beta$ 1, - $\beta$ 2, - $\beta$ 7 – as annotated previously for human CD94 [25]) forming a six-stranded anti-parallel  $\beta$ -sheet (Fig. 1C). CD94 and NKG2A each formed similar c-type lectin folds diverging most significantly from each other within the long loosely ordered loop 3 of NKG2A (NKG2A-L3) which did not form an ordered pair of anti-parallel  $\beta$ -strands (denoted CD94- $\beta$ 3, - $\beta$ 4) as observed in CD94 (Fig. 1D). The resulting assembly brought together a ligand binding site comprised of five CD94 loops (CD94-L2, -L3, -L5, -L6, -L7) and a  $\beta$ -strand (CD94- $\beta$ 6) combining with five NKG2A loops (NKG2A-L2, -L3, -L5, -L6, -L7) and two  $\beta$ -strands (NKG2A- $\beta$ 5, - $\beta$ 6) (Fig. 1E). A large portion of the binding site comprised of the long and largely disordered CD94-L3 and NKG2A-L3 loops which both, in our analyses, formed short  $\alpha$ -helices. To align to previously described human CD94 domain nomenclature, this helix (denoted CD94/NKG2A- $\alpha$ 2) is located within -L3 and thus divides loop 3 into -L3 and -L3', respectively (see Fig. 1C). Together, the mCD94–NKG2A complex formed 159 total contacts to Qa-1<sup>b</sup>-AL9, with the CD94 forming 54 non-bonded contacts, seven H-bonds and eight salt-bridges (total buried surface area of  $\sim 1100$  Å<sup>2</sup>) whilst the NKG2A formed 77 non-bonded contacts, 10 H-bonds and three salt-bridges (total buried surface area of 1300 Å<sup>2</sup>). As such, the recognition of Qa-1<sup>b</sup> appears evenly distributed across the heterodimeric receptor.

### Murine CD94–NKG2A engages Qa-1<sup>b</sup> similarly but with altered electrostatics

Given the debate as to the evolutionary origins of HLA-E and Qa-1<sup>b</sup>, comparison of CD94–NKG2A binding to their MHC ligands is important to understanding the conservation of receptor function between humans and mice used in pre-clinical studies. Overall comparison of mCD94–NKG2A binding to Qa-1<sup>b</sup> was performed with the previously published structures of the human CD94–NKG2A–HLA-E–VMA complex, PDB accession IDs: 3CDG and 3CII [26,27]. These human structures exhibit a high degree of similarity and were consequently treated equivalently during analysis and henceforth referred to as hCD94 and hNKG2A. Comparison with the human complex revealed the murine receptor bound with a conserved overall binding mode (Fig. 2A). Similar positioning of CD94–NKG2A to MHC ligand, as indicated by each subunits centre-of-mass (COM) was observed,

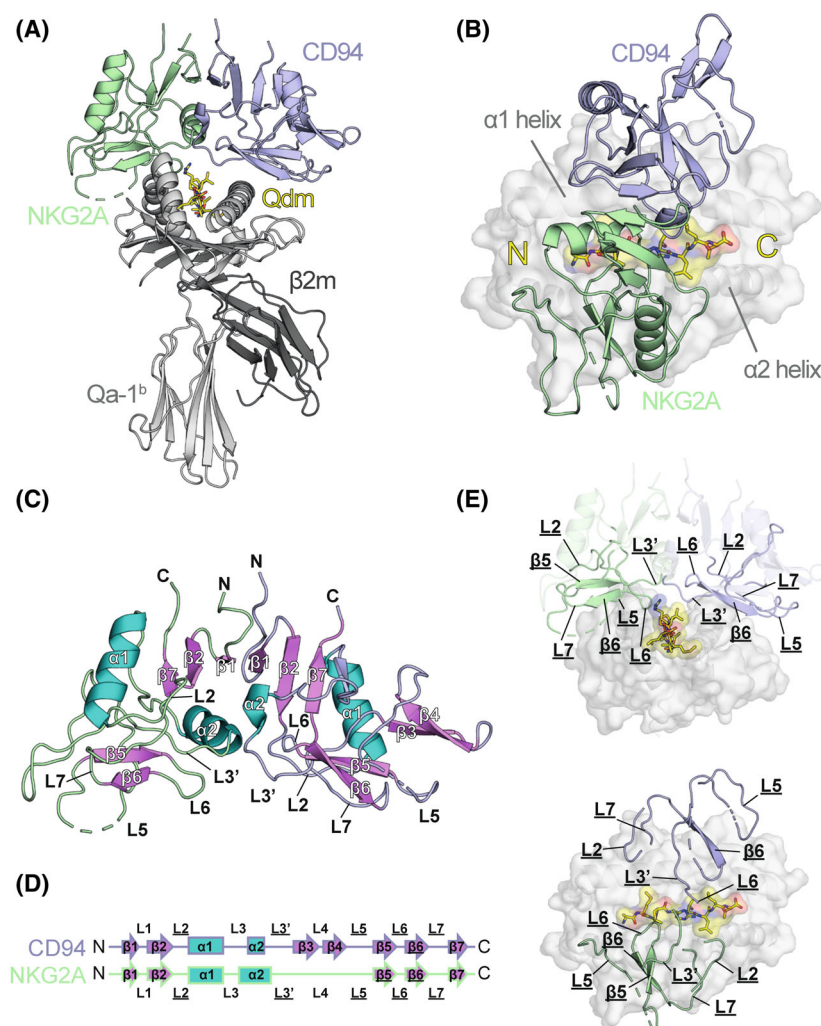


**Fig. 1.** Structure of murine CD94–NKG2A bound to Qdm presented by Qa-1<sup>b</sup>. (A) Structural overview of mCD94–NKG2A in complex with the Qdm peptide (AMAPRTLTL) presented by Qa-1<sup>b</sup>. CD94, NKG2A, Qa-1<sup>b</sup> and β2m represented as cartoon and coloured by chain; Qdm peptide = sticks, coloured by atom (carbon = yellow, oxygen = red, nitrogen = blue). (B) Birdseye view of mCD94–NKG2A binding atop the Qa-1<sup>b</sup> peptide binding groove. mCD94–NKG2A represented as cartoon with Qa-1<sup>b</sup> shown as a surface representation with MHCα1 and MHCα2 helices shown as cartoon representation. Qdm is shown as both sticks and surface and coloured by atom. (C) Cartoon representation of mCD94–NKG2A heterodimer domain architecture (N and C termini labelled N and C respectively). Structural elements annotated according to secondary structure; α-helices ([α] teal), β-strands ([β] magenta) and loops ([L], CD94 blue, NKG2A green). (D) Schematic representation of mCD94–NKG2A heterodimer domain architecture. Arrows = β-strands, rectangles = α-helices. Structural elements involved in ligand binding are underlined. (E) Arrangement of mCD94 and mNKG2A chains over Qa-1<sup>b</sup> (surface, α1 and α2 helices = cartoon) and Qdm peptide (surface and sticks) from side (top) and birds-eye (bottom) views. Each binding structural element is rendered opaque and non-binding elements semi-transparent. mCD94 is located over the Qa-1<sup>b</sup> α1 domain and Qdm P8 residue whilst NKG2A binds over the α2 domain and Qdm N-terminus resulting in a near perpendicular binding mode. Structural figures produced in PYMOL [49].

however, the murine receptor exhibited a more obtuse (3°) binding angle between dimer subunits (Fig. 2B). This increased angle was accompanied by small shifts (mNKG2A: 2.8 Å and mCD94: 3.4 Å) in overall positioning of the murine receptor; docking more centrally over the peptide binding groove of Qa-1<sup>b</sup>.

Alterations in the electrostatic surface potential of HLA-E and Qa-1<sup>b</sup> bound to their commonly presented MHC-I derived peptides (VMA and Qdm, respectively) have been previously documented and indicate divergence in HLA-E/Qa-1<sup>b</sup> structure–function [22]. HLA-E exhibits a largely negatively charged α2 helix



**Table 2.** Contacts between Qa-1<sup>b</sup> and CD94–NKG2A.

NKG2A	Qa-1 <sup>b</sup>	Type
Arg 146 <sup>Ne</sup>	Asp 151 <sup>Oδ1</sup>	Salt-bridge
Arg 146 <sup>Nη1</sup>	Glu 148 <sup>O</sup>	H-bond
Arg 146 <sup>Ne,Nη1</sup>	Asp 151 <sup>Oδ1,Oδ2</sup>	Salt-bridge
Arg 146 <sup>Cδ,Cζ</sup>	Ala 149 <sup>C,O</sup> Asp 151 <sup>Cδ</sup>	VDW
Ser 179 <sup>C,O</sup>	Gln 155 <sup>Ne2</sup>	VDW
Leu 180 <sup>N,Cα,C,O</sup>	Gln 155 <sup>Ne2</sup>	VDW
Ile 181 <sup>Cγ1,Cδ1</sup>	Asp 151 <sup>Cβ,O</sup> His 154 <sup>Cβ</sup> , Gln 155 <sup>Ne2,Cγ,N,Cδ,Oε1</sup>	VDW
Met 219 <sup>Cε</sup>	His 154 <sup>O</sup>	VDW
Ser 221 <sup>Cα,CCβ,Oγ</sup>	Gln 155 <sup>Oε1</sup> , Ala 158 <sup>Cβ</sup>	VDW
Ala 222 <sup>N</sup>	Gln 155 <sup>Oε1</sup>	H-bond
Ala 222 <sup>N,Cα,Cβ</sup>	Gln 155 <sup>Cδ,Oε1</sup>	VDW
Ser 223 <sup>O,Cβ,Oγ</sup>	Ala 158 <sup>C</sup> , Tyr 159 <sup>N,Cα,Cβ</sup> , Pro 163 <sup>Cγ,Cδ</sup>	VDW
Thr 226 <sup>Oγ1</sup>	Ala 158 <sup>Cα,Cβ</sup>	VDW
Asp 228 <sup>Oδ1,Oδ2</sup>	Arg 131 <sup>Nη1,Nη2</sup> Arg 157 <sup>Nη2</sup>	Salt-bridge
Asp 228 <sup>Cγ,Oδ1,Oδ2</sup>	Arg 131 <sup>Nη1,Nη2,Cζ</sup> , Arg 157 <sup>Nη2,Cζ</sup>	VDW
His 234 <sup>Cε1</sup>	His 154 <sup>Nδ1,Cε1,Ne2,Cδ2,Cγ</sup>	VDW
Pro 235 <sup>Cγ,Cδ</sup>	Asp 151 <sup>Oδ1,Oδ2</sup>	VDW
CD94	Qa-1 <sup>b</sup>	Type
Glu 79 <sup>Oε1,Oε2</sup>	Trp 65 <sup>Cβ,Cγ,Cδ2,Cε3</sup>	VDW
Phe 110 <sup>Cζ</sup>	Ala 149 <sup>O</sup>	VDW
Gln 112 <sup>O</sup>	Asn 73 <sup>Nδ2</sup>	H-bond
Gln 112 <sup>O,Cβ,Oε1,Ne2</sup>	Asn 73 <sup>Cγ,Oδ1,Nδ2</sup> , Glu 152 <sup>Oε1</sup>	VDW
Thr 113 <sup>Cα,Cβ,Oγ1,Cγ2</sup>	Asp 69 <sup>Cγ,Oδ2</sup> , Trp 65 <sup>Cζ2</sup>	VDW
Phe 114 <sup>N,O,Cβ,Cγ,Cδ1,Cδ2,Cε1,Cζ</sup>	Asp 69 <sup>Oδ1,Cγ,Cη2,Oδ1</sup> , Arg 72 <sup>Nη1,Cδ,CB</sup> , Asn 73 <sup>Cγ,Oδ1,Nδ2</sup>	VDW
Glu 143 <sup>Cδ,Oε1,Oε2</sup>	Arg 79 <sup>Ne,Cδ</sup>	VDW
Val 154 <sup>Cγ2</sup>	Arg 72 <sup>Cδ,Ne</sup>	VDW
Glu 164 <sup>Oε1</sup>	Arg 72 <sup>Nη2</sup>	Salt-bridge
Glu 164 <sup>Oε2</sup>	Arg 72 <sup>Ne,Nη2</sup>	Salt-bridge
Glu 164 <sup>Cδ,Oε2</sup>	Arg 72 <sup>Ne,Nη2,Cζ</sup>	VDW
Asn 168 <sup>Cγ,Nδ2</sup>	Arg 68 <sup>Nη1</sup>	VDW
Asn 170 <sup>Oδ1</sup>	Arg 72 <sup>Nη2</sup>	H-bond
Asn 170 <sup>Cγ,Oδ1,Nδ2</sup>	Arg 72 <sup>Nη2,Cζ</sup> , Trp 65 <sup>Cζ3,Cη2</sup>	VDW
Arg 171 <sup>Cγ,Cζ,Nη1,Nη2</sup>	Trp 65 <sup>Cη2,Cε2,Cζ2,Cδ1,Ne1</sup>	VDW
NKG2A	Peptide	Type
Ser 179 <sup>Oγ</sup>	Arg 5 <sup>Nη1</sup>	H-bond
Ser 179 <sup>O,Cβ,Oγ</sup>	Arg 5 <sup>Nη1,Cγ,Ne,Cζ,Cδ</sup>	VDW
Ala 222 <sup>O,Cβ</sup>	Pro 4 <sup>Cγ</sup> , Arg 5 <sup>Cδ,Cγ</sup>	VDW
Ser 223 <sup>Oγ</sup>	Pro 4 <sup>Cδ,Cγ</sup>	VDW
CD94	Peptide	Type
Phe 110 <sup>O</sup>	Arg 5 <sup>Nη1</sup>	H-bond
Phe 110 <sup>C,O</sup>	Arg 5 <sup>Nη1,CZ,Nη2</sup>	VDW
Gln 112 <sup>Oε1</sup>	Thr 6 <sup>N</sup>	H-bond
Gln 112 <sup>Ne2</sup>	Thr 6 <sup>O</sup>	H-bond
Gln 112 <sup>CA,Oε1,Ne2</sup>	Thr 6 <sup>O,N,Cγ2,C</sup> , Arg 5 <sup>Cα,C,Ne,Cζ,Nη2,Nη1</sup> , Cβ, Leu 8 <sup>Cγ</sup>	VDW
Ser 158 <sup>Oγ</sup>	Leu 8 <sup>Cδ1</sup>	VDW

and a pocket of positive charge in the α1 helix to which complementary charges are observed on the interfacing human CD94–NKG2A dimer surfaces ([26]

and Fig. 2C). In contrast, Qa-1<sup>b</sup> has an overall positively charged α2 helix; both in the unbound [22] and ligated state (Fig. 2C). Consequently, the murine

NKG2A interaction surface exhibits an overall negative charge (mCD94 = acidic, mNKG2A = acidic) – in contrast to the polarised human receptor (hCD94 = acidic, hNKG2A = basic). Thus, murine CD94–NKG2A utilises a highly acidic surface potential across its binding surface which complements the largely basic Qa-1<sup>b</sup> surface in comparison to human counterparts.

### Murine NKG2A exhibits a larger contribution to MHC binding than in humans

Given the differences in surface charge complementarity and receptor positioning between ligated human and murine CD94–NKG2A receptors, we next sought to quantify the contributions of both subunits of the CD94–NKG2A dimer to ligand binding between species. The interface areas of CD94–NKG2A and HLA-E/Qa-1<sup>b</sup> were similar, as observed by the total buried surface area (BSA) between the human and murine receptors (human = 2380 Å<sup>2</sup>, murine = 2400 Å<sup>2</sup>) (Fig. 2D). However, distribution of the interfaces across CD94 and NKG2A differed between the murine and the human, with the human interface biased towards CD94 and the murine interface spread more evenly between CD94 and NKG2A (Fig. 2D) (hCD94 : hNKG2A to pMHC = 60 : 40%; mCD94 : mNKG2A to pMHC = 54 : 46%). This difference in binding area distribution was most significant at the peptide interface. Both human and mouse peptide interfaces were skewed towards contacts to CD94. However, the CD94 bias was more notable in the human interface and not as marked in their murine counterparts (Fig. 2D).

Similar observations were also made by quantifying the contacts between CD94–NKG2A and MHC–peptide subunits whereby murine NKG2A formed an increased proportion (43% of total contacts, 12% increase vs. hNKG2A) of contacts most significantly to MHC (39% of total contacts, 10% increase vs. hNKG2A) (Fig. 2E). Increased contacts by mNKG2A included six salt bridges not observed in the human complex. The footprint of these contacts was more condensed around the peptide of Qa-1<sup>b</sup> by mCD94–NKG2A compared to that in humans (Fig. 2F) with CD94 distal from the locale of positions 19 and 89 which were contacted in the human system. Likewise, the increased contact footprint of mNKG2A differed most significantly through interactions with 157 and 159 in Qa-1<sup>b</sup>. Thus, in comparison to the human system, altered electrostatic complementarity is accompanied by an increased contribution of total mNKG2A contacts and more specific mNKG2A salt-bridge interactions to Qa-1<sup>b</sup>.

### Human and murine CD94–NKG2A are divergent at the ligand interface

Analysis of the global parameters of murine CD94–NKG2A binding to Qa-1<sup>b</sup> revealed that despite an overall similar binding mode, there was divergence of the biochemical properties of the receptor–ligand interface between species particularly with respect to NKG2A. Such differences coincide with the observation that murine CD94–NKG2A does not bind HLA-E, and human CD94–NKG2A does not bind Qa-1<sup>b</sup> [22]. Indeed, at the sequence level, murine and human NKG2A extracellular domains exhibit greater divergence (identity = 43%, similarity = 60%) compared to CD94 (identity = 54%, similarity = 71%) (Fig. 3A; Table 3). Similarly, the MHC-α2 helix, atop which NKG2A binds, exhibits greater divergence (identity = 58%, similarity = 67%) compared to MHC-α1 helix residues (identity = 70%, similarity = 78%) upon which CD94 binds.

In particular, a consecutive region encompassing -β5, -L6, -β6, which contributes a significant part of the ligand binding interface, exhibits particularly low sequence identity in both CD94 (38%, 5/13 residues) and NKG2A (25%, 3/12 residues). In mouse, mNKG2A diverges within this locale both sequentially and structurally, where the murine L6 loop is shifted 6.7 Å closer to the Qdm peptide cargo compared to the human complex structure (Fig. 3B). As a result, both A222 and S223 side chains contact Qdm at the P5 proline, which is common to both murine and human leader sequence peptides. Yet in the humans, V213 and N214, which occupy equivalent positions in the NKG2A–L6 loop, were too distal from the peptide to form contacts (Fig. 3B).

Murine NKG2A utilised two residues to form interactions with Qa-1<sup>b</sup> that are not observed in the human complex. Firstly, the guanidino group of mNKG2A R146 formed a salt bridge with the carboxyl group of D151 on the Qa-1<sup>b</sup> α2 helix (Fig. 3C). In humans, hNKG2A also possesses arginine at this position, however, HLA-E incorporates serine at position 151 and thus hNKG2A forms a hydrogen bond with S151 (Fig. 3C). Secondly, mNKG2A utilises the acidic D228 to form a salt bridge with R157 of Qa-1<sup>b</sup> (Fig. 3C). Interestingly, in humans, HLA-E also possesses R157, yet alanine occupies the equivalent position (A219) in NKG2A (Fig. 3C). As a result, hNKG2A does not contact HLA-E despite the salt-bridge capable R157 being similarly available for binding. Thus, the mNKG2A component of the CD94–NKG2A heterodimer utilises salt bridges to enable increased complementarity to Qa-1<sup>b</sup> concurrently with a larger contribution to the interface area and overall contact distribution compared to human CD94–NKG2A.

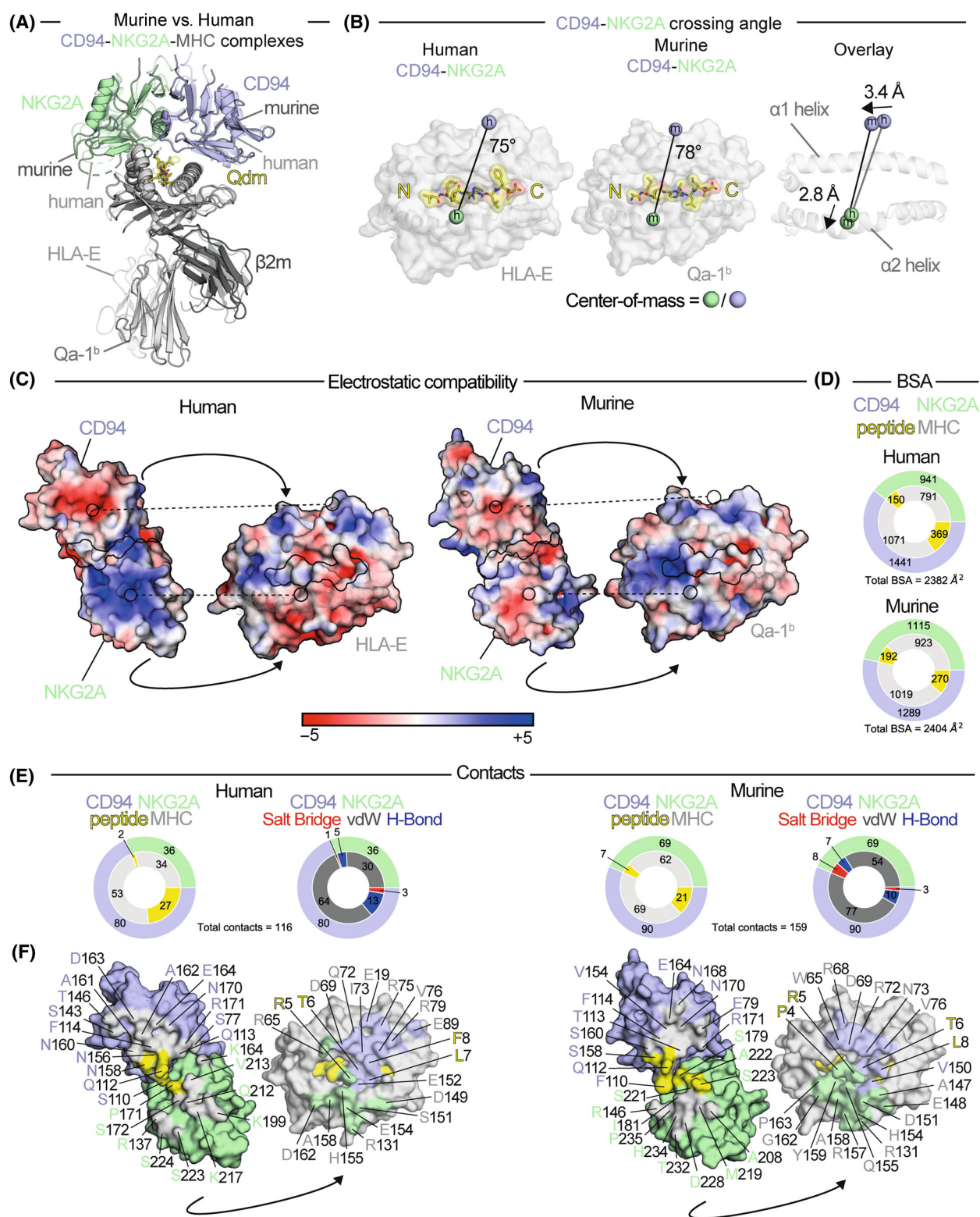


**Fig. 2.** Structural comparison of human and murine CD94–NKG2A binding to MHC ligand. (A) Structural alignment of mCD94–NKG2A and hCD94–NKG2A complexed with Qa-1<sup>b</sup>-Qdm and HLA-E-VMA, respectively. Murine and human structures coloured by chain, human structure rendered with transparency. (B) Conservation of cross-species binding mode as indicated by CD94 and NKG2A overall positioning (centre-of-mass (COM); spheres; coloured by chain) above the peptide (surface and sticks) and MHC (surface). A small rotation (3°) in the resulting crossing angle, in relation to the peptide binding groove, is exhibited between homologues due to 3.4 and 2.8 Å shifts in CD94 and NKG2A subunit COMs, respectively. (C) Human and murine CD94–NKG2A engage MHC via altered electrostatic complementarity. For each complex, the interface has been opened to show the underside of CD94–NKG2A and the MHC peptide binding groove surface that makes up the interface. Surfaces are coloured by electrostatic potential (scaled from +5 to –5 kT/e). (D) Human/murine CD94 and NKG2A subunit contributions to MHC and peptide buried surface area (BSA). Data presented as a nested donut chart whereby BSA of CD94 and NKG2A are quantified in the outer circle and sub-divided into their MHC or peptide interface partner (inner circle). Slice colours indicate protein chain. (E) The number of CD94–NKG2A subunit contacts to MHC and peptide in human and murine complexes (< 4.0 Å) (outer circle). Number of van der Waals (vdW; grey; < 4.0 Å), salt bridges (red; < 3.4 Å) and hydrogen bonds (blue; < 3.4 Å) are shown (inner circle). (F) Interface contacts between human (left) and mouse (right) CD94 (light blue) NKG2A (light green), HLA-E/Qa-1<sup>b</sup> (light grey) and peptide (yellow). The interface surfaces have been opened up as in (C), residues involved at the contact interface are cross-coloured to the corresponding binding subunit. Residues with contacts ≤ 4.0 Å are shown. Residues which contact multiple subunits are clarified in Fig. 3A. Structural figures produced in PYMOL.

### Qa-1<sup>b</sup> can be mutated to permit human CD94–NKG2A recognition

Despite the finding that mouse and human CD94–NKG2A utilise a unique molecular footprint, there is a similar position of the receptor over the  $\alpha 1$  and  $\alpha 2$  helices of their respective ligands (Fig. 2A). However, there are several divergent amino acids between Qa-1<sup>b</sup> and HLA-E at the interface involved in binding to CD94–NKG2A (Fig. 3A). Therefore, we made several mutations in Qa-1<sup>b</sup> to positions involved in binding mouse CD94–NKG2A to the corresponding amino acids present in HLA-E; namely Qa1<sup>b</sup>-W65R, -R72Q, -N73I, -D151S, -H154E, -Q155H and D162G (Fig. 4A,B). We then determined the ability of these mutants to bind to human and mouse CD94–NKG2A by surface plasmon resonance (SPR) (Fig. 4A).

The affinities of wild-type Qa-1<sup>b</sup> of  $K_D \sim 19 \mu\text{M}$  for mouse CD94–NKG2A and HLA-E of  $K_D \sim 5 \mu\text{M}$  for human CD94–NKG2A were consistent with our previous findings (Fig. 4A, Table 4) [22]. In contrast, there was no binding evident between wild-type Qa-1<sup>b</sup> and human CD94–NKG2A, nor HLA-E and mouse CD94–NKG2A, also consistent with previous findings (Fig. 4A, Table 4). Interestingly, the mutations Qa-1<sup>b</sup>-W65R and -D151S (Fig. 4A) appeared to slightly improve the affinity for mouse CD94–NKG2A, although there was minimal binding of both complexes with human CD94–NKG2A (Fig. 4A, Table 4). The mutations Qa-1<sup>b</sup>-H154E and -Q155H had a small impact (< 2-fold decrease in affinity) on binding to mouse CD94–NKG2A, whilst still not significantly interacting with human CD94–NKG2A. However, the mutant Qa-1<sup>b</sup>-N73I complex had a > 3-fold weaker affinity for mouse CD94–NKG2A and also had a weak but measurable affinity for human CD94–NKG2A (Fig. 4A, Table 4).

As W65R improved binding to mouse CD94–NKG2A and N73I improved binding to human CD94–NKG2A, a Qa-1<sup>b</sup> double mutant of W65R + N73I was generated to determine if this complex could interact with both mouse and human CD94–NKG2A. Intriguingly, SPR analysis showed the Qa-1<sup>b</sup> W65R + N73I mutant had the highest affinity of all the Qa-1<sup>b</sup> complexes for both mouse and human CD94–NKG2A (Fig. 4A, Table 4).

Qa-1<sup>b</sup>-W65 was bound by a cluster of murine CD94 loops (L2, L3' and L7) with diverse physicochemical side chains including the acidic E79 located on the L2 loop (Fig. 4C); where E79 charge complementarity with mutated W65R may have mediated enhanced murine CD94–NKG2A binding. In the human system, R65 on HLA-E is positioned in an apparent charge repulsion state within the basic NKG2A-K164 and CD94-R171 environment (Fig. 4C).

At position 73, Qa-1<sup>b</sup>-N73 forms a polar hydrogen bond network with Q112 and non-polar contacts with F114 of murine CD94 (Fig. 4D). Both Q112 and F114 are conserved in human CD94 (Fig. 3A) where HLA-E-I73 is less influential to the human CD94–NKG2A interface. Thus, a direct structural explanation for Qa-1<sup>b</sup>-N73I mutation-mediated binding to human CD94–NKG2A is not immediately clear. Nevertheless, our SPR analysis showed that adjustments could be made at the molecular interface to permit binding of a single complex to both mouse and human CD94–NKG2A.

### Discussion

The murine immune system is the most closely studied next to the human immune system. As a generalisation, fundamental principles gleaned from one species



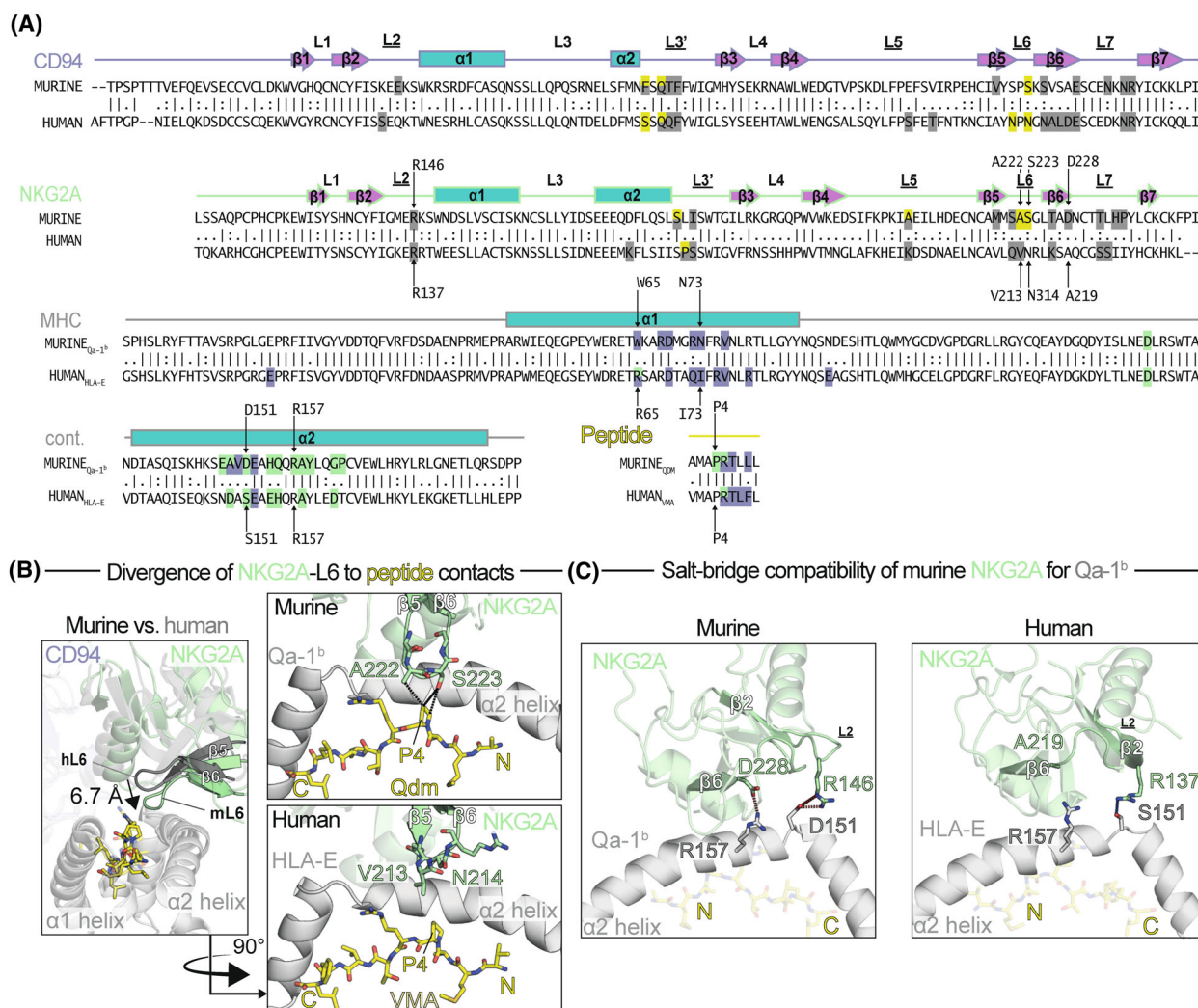


**Fig. 3.** Complementarity of murine CD94–NKG2A for Qa-1<sup>b</sup>. (A) Pairwise sequence alignment of human and murine CD94, NKG2A, Qa-1<sup>b</sup>/HLA-E and Qdm/VMA peptides. Schematic structural elements are shown as described in Fig. 1D. Residues which contact receptor/ligand are coloured with interacting subunit as described in Fig. 2F. Residues discussed in (B) and (C) are denoted with arrowed markers. “-” = gap, “.” = small positive score, “:” = score >1.0, “|” = identity. (B) Divergence of the murine NKG2A-L6 loop compared to the human complex. The murine complex is coloured as Fig. 1A and the human complex grey-scaled. (C) Salt-bridge compatibility of murine NKG2A for Qa-1<sup>b</sup>. Left: murine D228 and R146 of mNKG2A form high-enthalpy salt bridges to D151 and R157 of Qa-1<sup>b</sup>. Right: R137 and A219 in equivalent positions of hNKG2A are highlighted. R137 forms hydrogen bond with S151 whereas A219 does not bind R157. Structural figures produced in PYMOL. Aligned sequences of the murine and human CD94 and NKG2A extracellular domains: mCD94 = Uniprot: [O54707](#) [43–179], mNKG2A = Uniprot: [Q9Z202](#) [119–244], hCD94 = Uniprot: [Q13241](#) [43–179] & hNKG2A = Uniprot: [P26715](#) [110–233]. Murine and human MHC-1b sequences were: Qa-1<sup>b</sup> (H2-T23) = Uniprot: [P06339](#) [21–205] & HLA-E = Uniprot: [P13747](#) [22–206]. Sequences were aligned using the EMBOSS Needle Pairwise Sequence Alignment tool implementing the BLOSUM62 matrix [55].

transfer analogously to the other, yet the finer details often differ. The CD94/NKG2A interaction with Qa-1<sup>b</sup> is an ancient system whose primary function has been conserved, yet important differences remain [28,29]. In this study, we provide the crystal structure of the murine CD94/NKG2A–Qa-1<sup>b</sup> complex. This provides a direct comparison with the human

equivalent and provides a basis to rationalise the subtle differences between the two systems.

Despite similar presentation of the MHC leader sequence peptide, there is no cross-species reactivity between the CD94/NKG2A with the Qa-1<sup>b</sup>/HLA-E of mouse and human [22]. We show that this is primarily driven by the differences in charge distribution across

**Table 3.** Sequence similarity and identity of human and murine CD94–NKG2A/MHC1b extracellular domains.

Subunit	Murine	Human	% Similarity	% identity
MHC	Qa-1 <sup>b1</sup>	HLA-E <sup>2</sup>	80	70
α1			78	70
α2			67	58
CD94	mCD94 <sup>3</sup>	hCD94 <sup>4</sup>	71	54
NKG2A	mNKG2A <sup>5</sup>	hNKG2A <sup>6</sup>	60	43
Peptide	Qdm (H-2D3 <sub>3–11</sub> )	VMA(HLA-G <sub>3–11</sub> )	78	78

<sup>1</sup>Qa-1<sup>b</sup> (H2-T23) = Uniprot: [P06339](#) [21–205], α1 = [69–105], α2 = [157–201]; <sup>2</sup>HLA-E = Uniprot: [P13747](#) [22–206], α1 = [70–106], α2 = [158–202]; <sup>3</sup>mCD94 = Uniprot: [O54707](#) [43–179]; <sup>4</sup>hNKG2A = Uniprot: [Q9Z202](#) [119–244]; <sup>5</sup>hCD94 = Uniprot: [Q13241](#) [43–179]; <sup>6</sup>hNKG2A = Uniprot: [P26715](#) [110–233].

the interfaces. The murine interface is distinctly polar with the CD94 and NKG2A carrying net negative charges that complement positive patches on the Qa-1<sup>b</sup> molecule. By contrast, the human system is dipolar with the CD94 carrying a negative charge and the NKG2A a positive charge, with each binding oppositely charged regions on HLA-E [26]. The net result is that of the interactions to Qa-1<sup>b</sup> only one is strictly conserved to HLA-E (Q112<sup>CD94</sup> to E152<sup>HLA-E/Qa1<sup>b</sup></sup>). And yet through the mutation of Qa-1b residues W65 + N73, binding to the human CD94–NKG2A was attained. Interestingly, the double-substitution W65R + N73I also increased the affinity to mCD94–NKG2A beyond that of the wild-type. This is despite the single substitutions significantly reducing the recognition of Qa-1<sup>b</sup> by mCD94–NKG2A. Given the lack of inter-species cross recognition, it is unlikely that the Qa-1<sup>b</sup> W65 + N73 hybrid recapitulates either the docking mode to Qa-1<sup>b</sup> or HLA-E but instead represents an intermediate, suggestive of a degree of plasticity at the CD94–NKG2A interface. Taken together, the recognition of Qa-1<sup>b</sup> and HLA-E by CD94/NKG2A has substantially diverged but can be engineered for cross-reactivity.

CD94–NKG2A has a restricted peptide sequence preference with minimal modifications permitted from the canonical MHC-I leader peptide [30,31]. These restrictions are largely due to the specificity imposed on the peptide by MHC-E, with non-canonical peptides showing greatly reduced or intermediate affinity for the MHC [31–34]. The sequence of MHC-E varies across mammalian species, yet the sequences of the leader peptides are highly conserved such that Qa-1b can present the MHC-I leader sequences from other mammalian species, including human [32,35]. Similarly, the Qdm peptide can be presented by HLA-E and is recognised by hCD94–hNKG2A [36]. This is consistent with the notion of CD94–NKG2A co-

evolving with MHC-E whilst the MHC-I leader peptide remains conformationally fixed. Indeed, Q112<sup>CD94</sup> is the only strictly conserved interface residue, serving as the crucial anchor for both human and mouse receptors to the peptide. Our structural analysis supports the expectation that mCD94–mNKG2A would exhibit a comparable permissiveness to MHC-I leader sequences as observed in hCD94–hNKG2A. The murine structure reveals no steric barriers to slight alterations in the MHC leader peptide, such as phenylalanine at P8, present in some human MHC leader peptides, but not in murine counterparts.

The binding to Qa-1<sup>b</sup> is more evenly distributed between the CD94 and NKG2A domains than observed in the human which is heavily skewed towards the CD94 domain. Indeed, previous alanine scanning mutagenesis of the human NKG2A interface residues did not perturb the interaction with HLA-E [26]. Differences between the mouse and the human CD94/NKG2 system are also coincident with the swapping of the activating signalling domains. In the mouse the activating DAP10 and DAP12 adapters couple with the CD94 subunit, whilst in the human system DAP12 couples NKG2C and NKG2E [37]. As such, though the murine CD94/NKG2A/DAP12 complex is potentially bifunctional it appears to be predominantly inhibitory [37], and the NKG2C and NKG2E components do not contain any signalling capacity but are activating by virtue of CD94 adaptor coupling. In contrast, the human system is unequivocally binary with inhibitory NKG2A (ITIM domains) and activating NKG2C and NKG2E (coupling DAP12) [38]. This is consistent with a model whereby the role of human CD94 is to drive the interaction with HLA-E, whilst the NKG2 domain determines the downstream function of the receptor. Indeed, there are no differences between binding residues of human NKG2A and -2C. In contrast, there are subtle differences between murine NKG2A and -2C at the binding interface with a substitution at I181V. As murine NKG2A and CD94 share contributions to both pMHC recognition and signalling, such differences may be amplified through peptide specificity and underlie subtleties in pMHC recognition and downstream effector function and licensing of murine NK cells.

The CD94/NKG2A interaction with Qa-1<sup>b</sup> regulates both the adaptive and innate immune response. These functions are of interest in tumour studies where elevated Qa-1<sup>b</sup>/HLA-E expression is correlated with a negative prognosis [17,21,39]. Qa-1<sup>b</sup>/HLA-E expression is generally low in healthy tissue, yet becomes elevated in the inflammatory tumour environment. Thus, a

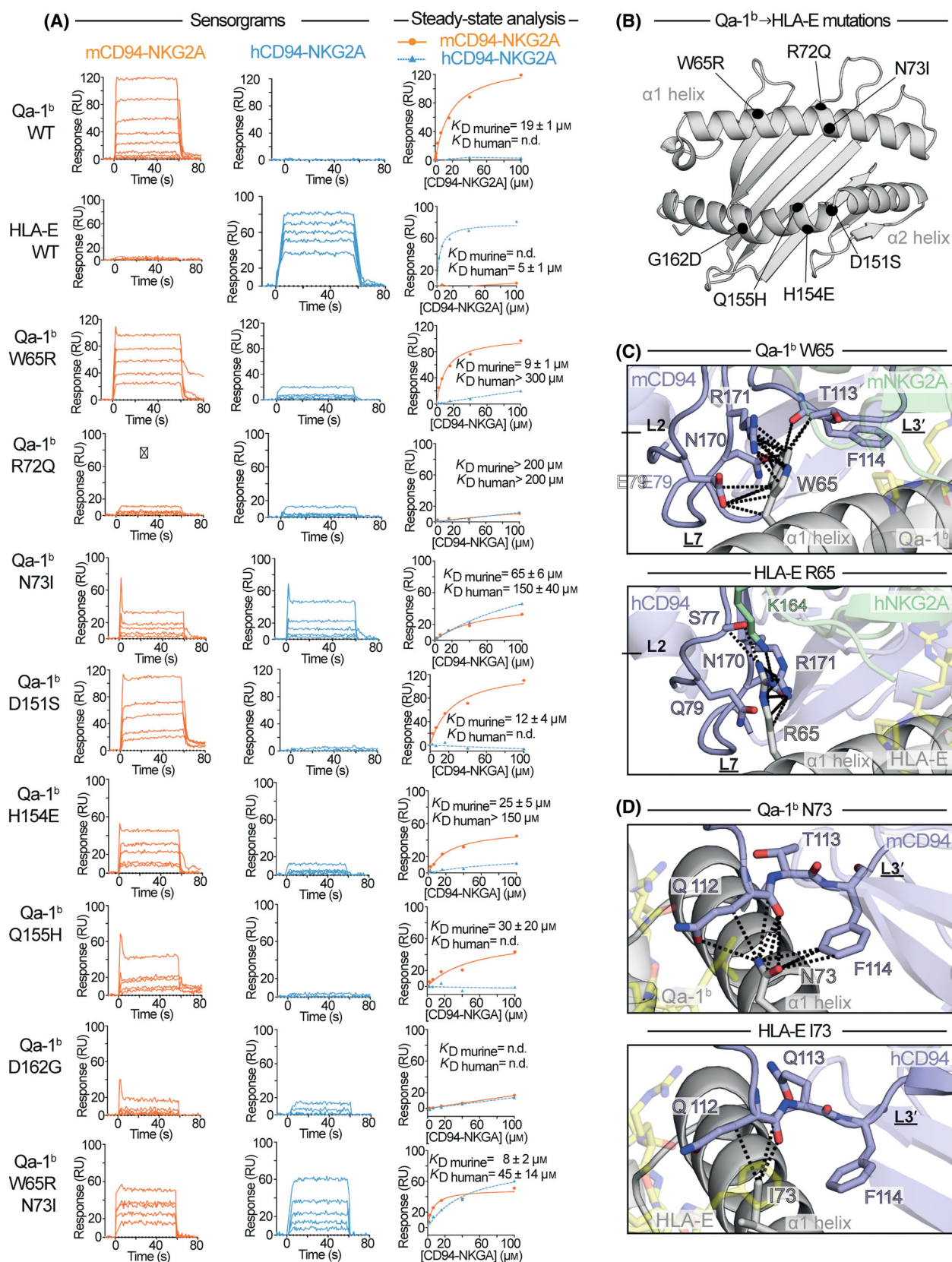




**Fig. 4.** Surface plasmon resonance of murine and human CD94–NKG2A interactions with Qa-1<sup>b</sup>. (A) Surface plasmon resonance measurements of murine and human CD94–NKG2A (m942A and h942A) binding to Qa-1<sup>b</sup> wild-type (WT) and named mutants. Representative reference subtracted sensorgrams shown. Equilibrium binding analysis with mean response at each analyte concentration for murine CD94–NKG2A (orange) and human CD94–NKG2A (blue) and a non-linear regression curve fitted to a one-to-one specific binding model (line) are shown. Calculated KD value  $\pm$  standard deviation is denoted inset. Calculated KD values derived from  $n = 2$  injections and representative of  $n = 2$  independent experiments. (B) Positions of the mutations to murine Qa-1<sup>b</sup> to approximate human HLA-E as tested by SPR mapped to the structure of Qa-1<sup>b</sup>. (C) The local environment of the Qa-1<sup>b</sup> residue W65 and the human HLA-E residue R65 at the interface with CD94–NKG2A, coloured by chain. (D) The local environment of the Qa-1<sup>b</sup> residue N73 and the human HLA-E residue I73 at the interface with CD94, coloured by chain. Structural figures produced in PYMOL.

**Table 4.** Summary of Qa-1<sup>b</sup> mutations that affected binding to murine and human CD94–NKG2A.

Qa-1 <sup>b</sup> /HLA-E complex	K <sub>D</sub> mouse CD94–NKG2A ( $\mu$ M)	K <sub>D</sub> human CD94–NKG2A ( $\mu$ M)
Qa-1 <sup>b</sup> Qdm wild type	19 $\pm$ 1	n.d.
HLA-E VMAPRTLLL	N/A	5 $\pm$ 1
Qa-1 <sup>b</sup> W65R	9 $\pm$ 1	> 300
Qa-1 <sup>b</sup> R72Q	n.d.	n.d.
Qa-1 <sup>b</sup> N73I	65 $\pm$ 6	150 $\pm$ 40
Qa-1 <sup>b</sup> D151S	12 $\pm$ 4	N/A
Qa-1 <sup>b</sup> H154E	33 $\pm$ 7	> 150
Qa-1 <sup>b</sup> Q155H	30 $\pm$ 20	n.d.
Qa-1 <sup>b</sup> D162G	N/A	N/A
Qa-1 <sup>b</sup> W65R + N73I	8 $\pm$ 2	45 $\pm$ 14

common tumour immune-evasion strategy involves the down-regulation of MHC-Ia expression to evade T-cell detection and upregulation of Qa-1<sup>b</sup>/HLA-E to dampen the NK cell response [21,40]. Thus, blocking the CD94–NKG2A–HLA-E interaction is a current target for several immune-therapy approaches [20,41,42]. Our data highlights that whilst the primary function of CD94/NKG2A is evolutionarily conserved there are nonetheless differences that may need to be considered when considering the murine model in relation to human immunotherapy.

## Materials and methods

### Recombinant protein production and purification

The extracellular domains of the heavy chain of Qa-1<sup>b</sup> (Uniprot: P06339 [21–300]), murine  $\beta$ 2-microglobulin (Uniprot: P01887 [21–119]), CD94 (Uniprot: O54707 [43–179]) and NKG2A (Uniprot: Q9Z202 [119–244]) were sub-cloned into the pET30 expression vector. Qa-1<sup>b</sup> was purified by established methods [22]. Briefly, the Qa-1<sup>b</sup> heavy chain and  $\beta$ 2m were expressed separately in *E. coli* into inclusion bodies. Qa-1<sup>b</sup> was refolded in the presence of the Qdm peptide (H-2D<sub>3-11</sub>: AMAPRTLLL) at a molar ratio of heavy chain :  $\beta$ 2m : peptide of 1 : 2 : 10 in a buffer comprised of 10 mM Tris pH 8.0, 400 mM L-arginine, 5 mM reduced glutathione,

and 0.5 mM oxidised glutathione. The refolded Qa-1<sup>b</sup> was subsequently dialysed into a buffer composed of 10 mM Tris pH 8.0 and then purified in turn by anion exchange then gel filtration chromatography and stored in 10 mM Tris pH 8.0, 150 mM NaCl. The CD94/NKG2A heterodimer was purified as described previously [26]. Components were expressed separately in *E. coli* from which inclusion bodies were isolated. These were resuspended in 8 M urea, 0.5 mM EDTA, and 1 mM DTT. CD94–NKG2A was refolded by flash dilution in a solution containing 5 M urea, 100 mM Tris–HCl (pH 8.0), 400 mM L-arginine, 5 mM reduced glutathione, and 0.5 mM oxidised glutathione. The refolding solution was then dialysed against 1 M urea and 10 mM Tris–HCl pH 8.0, followed by dialysis against 10 mM Tris–HCl pH 8.0. Refolded CD94–NKG2A heterodimer was then purified by anion exchange and size exclusion chromatography.

### Crystallisation and structure determination

The CD94–NKG2A/Qa-1<sup>b</sup>-AMAPRTLLL complex was generated by mixing the components at a 1 : 1 molar ratio and then concentrating to  $\sim 10$  mg·mL<sup>−1</sup>. Crystallisation was performed at 294 K by the hanging-drop vapour-diffusion method from a solution comprising 23% PEG3350 and 0.2 M NaBr. The structure was determined as detailed previously [43]. Prior to data collection, crystals were equilibrated in reservoir solution with 35% PEG3350 as a cryoprotectant and then flash-cooled in a stream of liquid nitrogen at 100 K. X-ray diffraction data were collected at the MX2 beamline (Australian Synchrotron, Clayton, Vic., Australia). The data were recorded on a Quantum-315 CCD detector and were integrated and scaled using MOSFLM and SCALA from the CCP4 programme suite [44]. Details of the data processing statistics are summarised in Table 1. Phases for the structure were determined by molecular replacement as implemented in PHASER [45] with the human CD94–NKG2A complex (Protein Data Bank accession code: PDB: 3BDW [24]) and Qa-1<sup>b</sup> (Protein Data Bank accession code: PDB: 3VJ6 [22]) used as independent search models. Refinement of the models proceeded with iterative rounds of manual building in COOT [46], refinement in BUSTER version 2.10.3 [47] and validation with MOLPROBITY [48]. The final model comprised the complete extracellular domains of Qa-1<sup>b</sup> (residues 1–278) and



b2m (residues 1–99). CD94 and NKG2A both were missing residues in the L5 loop; CD94 (residues 58–140, 147–178) and NKG2A (residues 127–208, 213–243). Refinement statistics are summarised in Table 1. Final model and data are submitted in the Protein databank under accession code PDB: 8UMO.

Visualisations of structures generated using PYMOL v2.2 [49]. Receptor crossing angle was derived by first calculating two vectors: (a) between CD94 and NKG2A centre-of-masses (calculated in PYMOL) and (b) a single-value decomposition (numpy.linalg.svd) [50] line-of-best-fit through MHC  $\alpha$ -helical C $\alpha$  atom coordinates (residues 49–85 137–181). Crossing angle was subsequently calculated by taking the arccosine of the dot product of both unit vectors. Surface electrostatics were calculated using PDB2PQR [51] and APBS [52]. Buried surface area (BSA) calculated using PISA [53] with default probe parameters. Intermolecular contacts enumerated using NCOT (CCP4) [44] with a 4.0 Å cut-off for all contact types. Subsequent graphs and plots generated using MATPLOTLIB [54].

### Surface plasmon resonance

Surface plasmon resonance (SPR) was performed essentially as described [22]. Briefly, all experiments were performed using a Bio-Rad ProteOn XPR36 instrument (BioRad, Hercules, CA, USA) at 25 °C in a buffer containing 10 mM HEPES (pH 7.4), 150 mM NaCl, and 0.05% Tween-20 (HBS-T). Mouse or human CD94–NKG2A was diluted into 10 mM sodium acetate (pH 5) and 60–450 response units (RU) were immobilised on separate flow cells of a GLC Sensorchip (Bio-Rad) by amine coupling, with an activated and deactivated adjacent flow cell with no coupled protein serving as a control. Recombinant Qa-1<sup>b</sup> and HLA-E were purified by size exclusion chromatography within 48 h prior to SPR. Wild type or mutant Qa-1<sup>b</sup> or wild type HLA-E (refolded with VMAPRTLTL peptide) was serially diluted in HBS-T and injected at a flow rate of 30  $\mu\text{L}\cdot\text{min}^{-1}$  for 60 s. Following subtraction of data from control flow cells, the steady-state  $K_D$  values were derived by the equilibrium fit option of the PROTEON software (BioRad, Hercules, CA, USA) and PRISM (GRAPHPAD PRISM software version 8.31, GraphPad Software, San Diego, CA, USA).

### Acknowledgements

This research was undertaken in part using the MX2 beamline at the Australian Synchrotron, part of ANSTO, and made use of the Australian Cancer Research Foundation (ACRF) detector. JR is supported by an NHMRC investigator award (2008981). JPV is supported by a Victorian Cancer Agency Fellowship (MCRF20043). Open access publishing facilitated by Monash University, as part of the Wiley - Monash

University agreement via the Council of Australian University Librarians.

### Conflict of interest

The authors declare no conflict of interest.

### Author contributions

Conception and design of the study by AGB, JR and JPV. Structural biology work designed and produced by BJM and JPV. Structural analysis by BJM and JPV. Surface plasmon resonance performed by LCS and AGB. BJM, LCS, AGB, JR and JPV contributed to data analysis and writing of the manuscript.

### Data availability statement

The structural data that support these findings are openly available in the wwPDB at <https://doi.org/10.2210/pdb8UMO/pdb>.

### References

- 1 Staub E, Rosenthal A & Hinzmann B (2004) Systematic identification of immunoreceptor tyrosine-based inhibitory motifs in the human proteome. *Cell Signal* **16**, 435–456.
- 2 Borrego F, Ulbrecht M, Weiss EH, Coligan JE & Brooks AG (1998) Recognition of human histocompatibility leukocyte antigen (HLA)-E complexed with HLA class I signal sequence-derived peptides by CD94/NKG2 confers protection from natural killer cell-mediated lysis. *J Exp Med* **187**, 813–818.
- 3 Moser JM, Gibbs J, Jensen PE & Lukacher AE (2002) CD94–NKG2A receptors regulate antiviral CD8(+) T cell responses. *Nat Immunol* **3**, 189–195.
- 4 Karre K, Ljunggren HG, Piontek G & Kiessling R (1986) Selective rejection of H-2-deficient lymphoma variants suggests alternative immune defence strategy. *Nature* **319**, 675–678.
- 5 Braud VM, Allan DS, O'Callaghan CA, Soderstrom K, D'Andrea A, Ogg GS, Lazetic S, Young NT, Bell JI, Phillips JH *et al.* (1998) HLA-E binds to natural killer cell receptors CD94/NKG2A, B and C. *Nature* **391**, 795–799.
- 6 Khalturin K, Becker M, Rinkevich B & Bosch TC (2003) Urochordates and the origin of natural killer cells: identification of a CD94/NKR-P1-related receptor in blood cells of *Botryllus*. *Proc Natl Acad Sci USA* **100**, 622–627.
- 7 Wroblewski EE, Parham P & Guethlein LA (2019) Two to tango: Co-evolution of hominid natural killer cell receptors and MHC. *Front Immunol* **10**, 177.

- 8 Vance RE, Kraft JR, Altman JD, Jensen PE & Raulet DH (1998) Mouse CD94/NKG2A is a natural killer cell receptor for the nonclassical major histocompatibility complex (MHC) class I molecule Qa-1(b). *J Exp Med* **188**, 1841–1848.
- 9 Joncker NT & Raulet DH (2008) Regulation of NK cell responsiveness to achieve self-tolerance and maximal responses to diseased target cells. *Immunol Rev* **224**, 85–97.
- 10 Braud V, Jones EY & McMichael A (1997) The human major histocompatibility complex class Ib molecule HLA-E binds signal sequence-derived peptides with primary anchor residues at positions 2 and 9. *Eur J Immunol* **27**, 1164–1169.
- 11 Ulbrecht M, Martinozzi S, Grzeschik M, Hengel H, Ellwart JW, Pla M & Weiss EH (2000) Cutting edge: the human cytomegalovirus UL40 gene product contains a ligand for HLA-E and prevents NK cell-mediated lysis. *J Immunol* **164**, 5019–5022.
- 12 Li F, Wei H, Wei H, Gao Y, Xu L, Yin W, Sun R & Tian Z (2013) Blocking the natural killer cell inhibitory receptor NKG2A increases activity of human natural killer cells and clears hepatitis B virus infection in mice. *Gastroenterology* **144**, 392–401.
- 13 Thimme R, Appay V, Koschella M, Panther E, Roth E, Hislop AD, Rickinson AB, Rowland-Jones SL, Blum HE & Pircher H (2005) Increased expression of the NK cell receptor KLRG1 by virus-specific CD8 T cells during persistent antigen stimulation. *J Virol* **79**, 12112–12116.
- 14 Sheu BC, Chiou SH, Lin HH, Chow SN, Huang SC, Ho HN & Hsu SM (2005) Up-regulation of inhibitory natural killer receptors CD94/NKG2A with suppressed intracellular perforin expression of tumor-infiltrating CD8<sup>+</sup> T lymphocytes in human cervical carcinoma. *Cancer Res* **65**, 2921–2929.
- 15 Bertone S, Schiavetti F, Bellomo R, Vitale C, Ponte M, Moretta L & Mingari MC (1999) Transforming growth factor-beta-induced expression of CD94/NKG2A inhibitory receptors in human T lymphocytes. *Eur J Immunol* **29**, 23–29.
- 16 Borst L, Sluijter M, Sturm G, Charoentong P, Santegoets SJ, van Gulijk M, van Elsas MJ, Groeneveldt C, van Montfoort N, Finotello F *et al.* (2022) NKG2A is a late immune checkpoint on CD8 T cells and marks repeated stimulation and cell division. *Int J Cancer* **150**, 688–704.
- 17 Gooden M, Lampen M, Jordanova ES, Leffers N, Trimbois JB, van der Burg SH, Nijman H & van Hall T (2011) HLA-E expression by gynecological cancers restrains tumor-infiltrating CD8(+) T lymphocytes. *Proc Natl Acad Sci USA* **108**, 10656–10661.
- 18 de Kruijf EM, Sajet A, van Nes JG, Natanov R, Putter H, Smit VT, Liefers GJ, van den Elsen PJ, van de Velde CJ & Kuppen PJ (2010) HLA-E and HLA-G expression in classical HLA class I-negative tumors is of prognostic value for clinical outcome of early breast cancer patients. *J Immunol* **185**, 7452–7459.
- 19 Salomé B, Sfakianos JP, Ranti D, Daza J, Bieber C, Charap A, Hammer C, Banchereau R, Farkas AM, Ruan DF *et al.* (2022) NKG2A and HLA-E define an alternative immune checkpoint axis in bladder cancer. *Cancer Cell* **40**, 1027–1043.e9.
- 20 André P, Denis C, Soulas C, Bourbon-Caillet C, Lopez J, Arnoux T, Bléry M, Bonnafous C, Gauthier L, Morel A *et al.* (2018) Anti-NKG2A mAb is a checkpoint inhibitor that promotes anti-tumor immunity by unleashing both T and NK cells. *Cell* **175**, 1731–1743.e13.
- 21 van Montfoort N, Borst L, Korner MJ, Sluijter M, Marijt KA, Santegoets SJ, van Ham VJ, Ehsan I, Charoentong P, Andre P *et al.* (2018) NKG2A blockade potentiates CD8 T cell immunity induced by cancer vaccines. *Cell* **175**, 1744–1755.e15.
- 22 Zeng L, Sullivan LC, Vivian JP, Walpole NG, Harpur CM, Rossjohn J, Clements CS & Brooks AG (2012) A structural basis for antigen presentation by the MHC class Ib molecule, Qa-1b. *J Immunol* **188**, 302–310.
- 23 Miller JD, Weber DA, Ibegbu C, Pohl J, Altman JD & Jensen PE (2003) Analysis of HLA-E peptide-binding specificity and contact residues in bound peptide required for recognition by CD94/NKG2. *J Immunol* **171**, 1369–1375.
- 24 Sullivan LC, Clements CS, Beddoe T, Johnson D, Hoare HL, Lin J, Huyton T, Hopkins EJ, Reid HH, Wilce MC *et al.* (2007) The heterodimeric assembly of the CD94–NKG2 receptor family and implications for human leukocyte antigen-E recognition. *Immunity* **27**, 900–911.
- 25 Boyington JC, Riaz AN, Patamawenu A, Coligan JE, Brooks AG & Sun PD (1999) Structure of CD94 reveals a novel C-type lectin fold: implications for the NK cell-associated CD94/NKG2 receptors. *Immunity* **10**, 75–82.
- 26 Petrie EJ, Clements CS, Lin J, Sullivan LC, Johnson D, Huyton T, Heroux A, Hoare HL, Beddoe T, Reid HH *et al.* (2008) CD94–NKG2A recognition of human leukocyte antigen (HLA)-E bound to an HLA class I leader sequence. *J Exp Med* **205**, 725–735.
- 27 Kaiser BK, Pizarro JC, Kerns J & Strong RK (2008) Structural basis for NKG2A/CD94 recognition of HLA-E. *Proc Natl Acad Sci USA* **105**, 6696–6701.
- 28 Joly E & Rouillon V (2006) The orthology of HLA-E and H2-Qa1 is hidden by their concerted evolution with other MHC class I molecules. *Biol Direct* **1**, 2.
- 29 Yeager M, Kumar S & Hughes AL (1997) Sequence convergence in the peptide-binding region of primate and rodent MHC class Ib molecules. *Mol Biol Evol* **14**, 1035–1041.
- 30 Huisman BD, Guan N, Rückert T, Garner L, Singh NK, McMichael AJ, Gillespie GM, Romagnani C &

- Birnbaum ME (2023) High-throughput characterization of HLA-E-presented CD94/NKG2x ligands reveals peptides which modulate NK cell activation. *Nat Commun* **14**, 4809.
- 31 Kraft JR, Vance RE, Pohl J, Martin AM, Raulet DH & Jensen PE (2000) Analysis of Qa-1(b) peptide binding specificity and the capacity of CD94/NKG2A to discriminate between Qa-1-peptide complexes. *J Exp Med* **192**, 613–624.
  - 32 DeCloux A, Woods AS, Cotter RJ, Soloski MJ & Forman J (1997) Dominance of a single peptide bound to the class I(B) molecule, Qa-1b. *J Immunol* **158**, 2183–2191.
  - 33 Hansen SG, Wu HL, Burwitz BJ, Hughes CM, Hammond KB, Ventura AB, Reed JS, Gilbride RM, Ainslie E, Morrow DW *et al.* (2016) Broadly targeted CD8<sup>+</sup> T cell responses restricted by major histocompatibility complex E. *Science* **351**, 714–720.
  - 34 Walters LC, Rozbesky D, Harlos K, Quastel M, Sun H, Springer S, Rambo RP, Mohammed F, Jones EY, McMichael AJ *et al.* (2022) Primary and secondary functions of HLA-E are determined by stability and conformation of the peptide-bound complexes. *Cell Rep* **39**, 110959.
  - 35 Kurepa Z, Hasemann CA & Forman J (1998) Qa-1b binds conserved class I leader peptides derived from several mammalian species. *J Exp Med* **188**, 973–978.
  - 36 Brooks AG, Borrego F, Posch PE, Patamawenu A, Scorzelli CJ, Ulbrecht M, Weiss EH & Coligan JE (1999) Specific recognition of HLA-E, but not classical, HLA class I molecules by soluble CD94/NKG2A and NK cells. *J Immunol* **162**, 305–313.
  - 37 Saether PC, Hoelsbrekken SE, Fossum S & Dissen E (2011) Rat and mouse CD94 associate directly with the activating transmembrane adaptor proteins DAP12 and DAP10 and activate NK cell cytotoxicity. *J Immunol* **187**, 6365–6373.
  - 38 Lanier LL, Corliss B, Wu J & Phillips JH (1998) Association of DAP12 with activating CD94/NKG2C NK cell receptors. *Immunity* **8**, 693–701.
  - 39 Andersson E, Poschke I, Villabona L, Carlson JW, Lundqvist A, Kiessling R, Seliger B & Masucci GV (2016) Non-classical HLA-class I expression in serous ovarian carcinoma: correlation with the HLA-genotype, tumor infiltrating immune cells and prognosis. *Oncotargets Ther* **5**, e1052213.
  - 40 Talebian Yazdi M, van Riet S, van Schadewijk A, Fiocco M, van Hall T, Taube C, Hiemstra PS & van der Burg SH (2016) The positive prognostic effect of stromal CD8<sup>+</sup> tumor-infiltrating T cells is restrained by the expression of HLA-E in non-small cell lung carcinoma. *Oncotarget* **7**, 3477–3488.
  - 41 Kamiya T, Seow SV, Wong D, Robinson M & Campana D (2019) Blocking expression of inhibitory receptor NKG2A overcomes tumor resistance to NK cells. *J Clin Invest* **129**, 2094–2106.
  - 42 Ruggeri L, Urbani E, Andre P, Mancusi A, Tosti A, Topini F, Blery M, Animobono L, Romagne F, Wagtman N *et al.* (2016) Effects of anti-NKG2A antibody administration on leukemia and normal hematopoietic cells. *Haematologica* **101**, 626–633.
  - 43 Rossmann MG (2001) Molecular replacement – historical background. *Acta Crystallogr D* **57**, 1360–1366.
  - 44 Collaborative Computational Project, Number 4 (1994) The CCP4 suite: programs for protein crystallography. *Acta Crystallogr D* **50**, 760–763.
  - 45 McCoy AJ (2007) Solving structures of protein complexes by molecular replacement with Phaser. *Acta Crystallogr D* **63**, 32–41.
  - 46 Emsley P & Cowtan K (2004) Coot: model-building tools for molecular graphics. *Acta Crystallogr D* **60**, 2126–2132.
  - 47 Blanc E, Roversi P, Vornrhein C, Flensburg C, Lea SM & Bricogne G (2004) Refinement of severely incomplete structures with maximum likelihood in BUSTER-TNT. *Acta Crystallogr D* **60**, 2210–2221.
  - 48 Davis IW, Leaver-Fay A, Chen VB, Block JN, Kapral GJ, Wang X, Murray LW, Arendall WB 3rd, Snoeyink J, Richardson JS *et al.* (2007) MolProbity: all-atom contacts and structure validation for proteins and nucleic acids. *Nucleic Acids Res* **35**, W375–W383.
  - 49 Delano WL (2002) The PyMOL Molecular Graphics System. DeLano Scientific, San Carlos, CA. <http://www.pymol.org>.
  - 50 Oliphant TE (2007) Python for scientific computing. *Comput Sci Eng* **9**, 10–20.
  - 51 Dolinsky TJ, Nielsen JE, McCammon JA & Baker NA (2004) PDB2PQR: an automated pipeline for the setup of Poisson-Boltzmann electrostatics calculations. *Nucleic Acids Res* **32**, W665–W667.
  - 52 Jurrus E, Engel D, Star K, Monson K, Brandi J, Felberg LE, Brookes DH, Wilson L, Chen J, Liles K *et al.* (2018) Improvements to the APBS biomolecular solvation software suite. *Protein Sci* **27**, 112–128.
  - 53 Krissinel E & Henrick K (2007) Inference of macromolecular assemblies from crystalline state. *J Mol Biol* **372**, 774–797.
  - 54 Hunter JD (2007) Matplotlib: a 2D graphics environment. *Comput Sci Eng* **9**, 90–95.
  - 55 Madeira F, Park YM, Lee J, Buso N, Gur T, Madhusoodanan N, Basutkar P, Tivey ARN, Potter SC, Finn RD *et al.* (2019) The EMBL-EBI search and sequence analysis tools APIs in 2019. *Nucleic Acids Res* **47**, W636–W641.